厚生労働科学研究費補助金（医療機器開発推進研究事業）

（分担）研究報告書

Si/CdTe検出器の改良と臨床用装置の開発に関する研究

（分担）研究者・三戸美生　株式会社アクロラド開発部長

研究要旨：小型で可搬性の高いコンプトンカメラ製作のために、テルル化カドミウム半導体を用いた両面ストリップ検出器の開発を行なった。この検出器の開発の成功により少ない読み出しチャンネル数の大面積ガンマ線イメージング装置が製作可能となった。

A．研究目的

半導体コプトンカメラのうちSi/CdTeを検出器として利用したものは、装置サイズとして小型の物が製作可能であると考えられる。そこで、可動性の高い可搬型簡易コンプトンカメラとしてSi/CdTeを用いたものをJAXAと共同で開発する。併せて、理化学研究所において小動物を用いた基礎実験を行うことで、動物実験における基礎データを収集し、装置改良に資する。

B．研究方法

小動物を用いた実測に向けて最適設計を行い、コンパクトなSi/CdTeコンプトンカメラシステムを臨床実験用に開発する。現時点で国内外を問わず、要求される性能を持つシステムを製作販売できる所は存在しないため、センサーのみならす、組み込み型高速データ収集システム、ハイテク素材を使った冷却システムなどをJAXAが構築する。また、構築したシステムを用いて理化学研究所の放射性同位元素使用施設における小動物による基礎実験を行う。

（倫理面への配慮）

本提案は、ラット、マウスなどの実験動物を使用する。研究の遂行にあたっては、（独）理化学研究所・動物実験実施規定に従い、動物実験計画を申請し、承認後に実験を遂行する。

C．研究結果

シリコン素子と組み合わせて実装されるCdTe素子の設計を行った。従来JAXAグループで進めてきたインジウム電極を用いた検出器ばかりではなく、新しくアルミニウムやニッケルを用いた検出器についても、単素子による基礎実験を行いながら研究を行った。また、インジウム電極を用いたCdTeイメージング検出器を実際のコンプトンカメラに組み込むために、性能評価をJAXAと共同で行なった。その結果、スペクトルから、半導体の中に発生するキャリアのモビリティ・寿命積を求める手法をJAXAにおいて、ソフトウェアパッケージとしてまとめ、株式会社アクロラドに技術移転した。
このソフトウェアを用いることにより、良質の結晶を製造するための条件出しが容易となり生産効率が向上した。

D．考察

世界ではじめてテルル化カドミウム半導体を用いた両面ストリップ検出器の開発に成功した。これは大面積のガンマ線イメージング装置に応用可能であると考えられる。

E．結論

テルル化カドミウム半導体を用いた両面ストリップ検出器の開発が成功したことにより、少ない読み出しチャンネル数で100ミクロン以下の位置分解能をもつ大面積ガンマ線検出器が実現したといえる。これは当初、計画には入っていなかった大きな伸展であり、事業化の鍵であるといえる。

G．研究発表

1．論文発表

(1) 玉城充、三戸美生、首藤 靖浩、山口 浩司、喜友名達也、山本雅也、寒河江健一、喜名徹、CdTeを用いたX線画像検出器モジュールの開発、日本放射線技術会　画像通信　Vol.30(2)、34-39、2007年

2．学会発表

(1) 三戸美生、首藤 靖浩、山口 浩司、喜友名達也、山本雅也、玉城充、寒河江健一、喜名徹、小泉達洋、CdTeを用いたX線画像検出器モジュールの開発、日本非破壊検査協会放射線分科会「放射線による非破壊評価シンポジウム」、東京都、2008年１月

H．知的財産権の出願・登録状況（予定を含む。）

1．特許取得
　なし

2．実用新案登録
　なし

3．その他
　なし

厚生労働科学研究費補助金（医療機器開発推進研究事業）

（分担）研究報告書

Ｇｅ検出器の開発に関する研究

（分担）研究者・鈴木孝宏　キャンベラジャパン株式会社技術部

研究要旨：撮像効率向上のために、2つの結晶間隔を、現有のプロトタイプGeコンプトンカメラより狭くした検出器を製作した。製作した検出器の個々のチャンネルは、コンプトンカメラとして使用するにあたり十分な性能を有していることを実測定により確認した。

Ａ．研究目的

Geコンプトンカメラに必要な２つの半導体検出器の配置の最適化を行い、撮像効率の向上を目指す。あわせて、撮像効率が最適となる配置における、撮像精度を評価する。

Ｂ．研究方法

シミュレーションにより、２つの検出器の間隔を、現有のプロトタイプコンプトンカメラ（ＧＲＥＩ）より狭くした場合でも、撮像精度に深刻な影響を与えないことを確認した。そこで、検出器間距離を狭くしたスタックストリップ型ゲルマニウム半導体検出器を製作し、実測定により個々のチャンネルの性能評価を行う。その後、小動物を用いた撮像実験を実施し、コンプトンカメラとしての総合的な性能評価を行う。

（倫理面への配慮）
本提案では、まだ動物実験を行っていない。

Ｃ．研究結果

キャンベラジャパン株式会社において、２つの結晶間隔を物理的に可能な限り狭くした(25 mm) Ge検出器を製作した。現有のプロトタイプ・コンプトンカメラＧＲＥＩ（結晶間隔 45 mm）と比較して結晶間距離を狭くした事により、２つ結晶間の電気的相互作用による性能劣化が懸念された。しかしながら、各ストリップ信号の実測定により、現有ＧＲＥＩと同等のエネルギー分解能である半値幅3.5 keV 以下（1332 keV、1000cps　入力カウント、シェイピングタイム４～６μｓ使用時）を有していることを確認した。

Ｄ．考察

今回製作した検出器は可能な限り２つのGe結晶間の距離を狭くした。しかしながら、25 mmという結晶間距離は、冷却用クライオスタット内の真空中にGe結晶を支持するために必要な物理的限界距離であり、電気的相互作用による性能劣化が起こりうる距離には達していないと考えられる。そのため、現有GREIと同等のエネルギー測定精度が得られたと考えられる。

今後、この検出器をコンプトンカメラとして用いた小動物実験等を実施し、撮像精度を確認する必要がある。

Ｅ．結論

結晶間隔を狭くした場合でも検出器として個々のチャンネルは性能上問題ない事を確認した。来年度、この検出器を用いて撮像実験を行い、コンプトンカメラとして、シミュレーション通りの撮像効率の向上が達成されているか、また撮像精度に問題がないか評価を行う。

Ｇ．研究発表

1.　論文発表
　　なし

2.　学会発表
　　なし

Ｈ．知的財産権の出願・登録状況（予定を含む。）

1. 特許取得
　　なし

2. 実用新案登録
　　なし

3. その他
　　なし

研究成果の刊行に関する一覧表

書籍

著者氏名	論文タイトル名	書籍全体の編集者名	書　籍　名	出版社名	出版地	出版年	ページ
榎本秀一	ミネラルのイメージング技術	糸川嘉則	ミネラルの科学と最新応用技術	シーエムシー出版			印刷中

雑誌

発表者氏名	論文タイトル名	発表誌名	巻号	ページ	出版年
Enomoto S.	Development of multi-elemental molecular imaging on semiconductor compton telescope as a tool for metallomics research	Pure and Applied Chemistry			in press
Motomura S., Kanayama Y., Haba H., Watanabe Y., and Enomoto S.	Multiple Nuclide Imaging in Live Mouse Using Semiconductor Compton Camera for Multiple Molecular Imaging	J. Anal. Atom. Spectrom.			in press
渡辺恭良、鈴木正昭、尾上浩隆、土居久志、和田康弘、片岡洋祐、榎本秀一	分子イメージング研究による創薬・疾患診断の革新（第44回（2007年度）ベルツ賞受賞論文）	日本医師会雑誌	136(12)	2469-2474	2008
渡辺恭良、鈴木正昭、尾上浩隆、土居久志、和田康弘、片岡洋祐、榎本秀一	分子イメージング研究による創薬・疾患診断の革新（第44回（2007年度）ベルツ賞受賞論文）	最新医学	63(1)	116-138	2008
Motomura S, Enomoto S, Haba H, Igarashi K, Gono Y, Yano Y.	Gamma-ray Compton imaging of multitracer in biological samples using strip germanium telescope	IEEE Trans. Nucl. Sci.	54(3)	710-717	2007

Y. Ishii, A. Toyoshima, K. Tsukada, M. Asai, H. Toume, I. Nishinaka, Y. Nagame, S. Miyashita, T. Mori, H. Suganuma, H. Haba, M. Sakamaki, S. Goto, H. Kudo, K. Akiyama, Y. Oura, H. Nakahara, Y. Tashiro, A. Shinohara, M. Schadel, W. Bruchle, V. Pershina, and J. V. Kratz	Fluoride Complexation of Element 104, Rutherfordium (Rf), Investigated by Cation-exchange Chromatography	Chem. Lett.	37(18)	288-289	2008
Yoshiro Yamashita, Yoshio Takahashi, Hiromitsu Haba, Shuichi Enomoto, Hiroshi Shimizu	Comparison of reductive accumulation of Re and Os in seawater - sediment systems	Geochimica et Cosmochimica Acta	71(14)	3458-3475	2007
M. Kidera, K. Takahashi, S. Enomoto, Y. Mitsubori, A. Goto, Y. Yano	Development of a novel mass spectrometer equipped with an electron cyclotron resonance ion source	European Journal of Mass Spectrometry	13(4)	239-248	2007
M. Kidera, K. Takahashi, S. Enomoto, A. Goto and Y. Yano	New fragment ion production method using super cold electrons in electron cyclotron resonance plasma	European Journal of Mass Spectrometry	13(5)	355-358	2007
R. Minayoshi, T. Ohyama, N. Kinugawa, J. Kamishima, T. Ogi, K. Ishikawa, M. Noguchi, H. Suganuma, K. Takahashi, S. Enomoto and M. Yanaga	Change of concentrations of trace elements and protein contents in the liver of zinc deficient mice	Journal of Radioanalytical and Nuclear Chemistry	272(2)	429-431	2007
五十嵐香織、金山 洋介、本村 信治、松田 芳和、榎本 秀一	牡蠣抽出物の胃液分泌能	Trace Nutrients Research	24	56-58	2007

Mizuno, K., Tanaka, M., Nozaki, S., Yamaguti, K., Mizuma, H., Sasabe, T., Sugino, T., Shirai, T., Kataoka, Y., Kajimoto, Y., Kuratsune, H., Kajimoto, O., and Watanabe, Y.	Mental fatigue-induced decrease in levels of several plasma amino acids	J. Neural Transm.	114	555-561	2007
Tamura, Y., Kataoka, Y., Cui, Y., Takamori, Y., Watanabe, Y., and Yamada, H.	Multi-directional differentiation of doublecortin- and NG2-immunopositive progenitor cells in the adult rat neocortex *in vivo*.	Eur. J. Neurosci.	25	3489-3498	2007
Tamura, Y., Kataoka, Y., Cui, Y., Takamori, Y., Watanabe, Y., and Yamada, H.	Intracellular translocation of glutathione S-transferase pi during oligodendrocyte differentiation in the adult rat cerebral cortex *in vivo*	Neuroscience	148	535-540	2007
Kishishita T., Ikeda H., Kiyuna T., Tamura K., Nakazawa K., Takahashi T.	Development of a low-noise analog front-end ASIC for CdTe detectors	Nuclear Instruments and Methods in Physics Research, Section A	580	1363-1371	2007
Takeda S., Watanabe S., Tanaka T., Nakazawa K., Takahashi T., Fukazawa Y., Yasuda H., Tajima H., Kuroda Y., Onishi M., Genba K.	Development of double-sided silicon strip detectors(DSSD) for a Compton telescope	Nuclear Instruments and Methods in Physics Research, Section A	579	859-865	2007

Watanabe S., Takeda S., Ishikawa S., Odaka H., Ushio M., Tanaka T., Nakazawa K., Takahashi T., Tajima H., Fukazawa Y., Kuroda Y., Onishi M.	Development of semiconductor imaging detectors for a Si/CdTe Compton camera	Nuclear Instruments and Methods in Physics Research, Section A	579	871-877	2007
Odaka H., Takeda S. Watanabe S., Ishikawa S., Ushio M., Tanaka T., Nakazawa K., Takahashi T., Tajima H., Fukazawa Y.	Performance study of Si/CdTe semiconductor Compton telescopes with Monte Carlo simulation	Nuclear Instruments and Methods in Physics Research, Section A	579	878-885	2007
Watanabe S., Ishikawa S.-N., Takeda S., Odaka H., Tanaka T., Takahashi T., Nakazawa, K., Yamazato, M., Higa, A., Kaneku, S.	New CdTe pixel gamma-ray detector with pixelated Al schottky anodes	Japanese Journal of Applied Physics Part 1	46(9A)	6043-6045	2007
H. Haba, D. Kaji, H. Kikunaga, T. Akiyama, N. Sato, K. Morimoto, A. Yoneda, K. Morita, T. Takabe, and A. Shinohara	Development of Gas-jet Transport System Coupled to the RIKEN Gas-filled Recoil Ion Separator GARIS for Superheavy Element Chemistry	J. Nucl. Radiochem. Sci.	8(2)	55-58	2007
玉城充、三戸美生、首藤 靖浩、山口 浩司、喜友名達也、山本雅也、寒河江健一、喜名徹	CdTeを用いたX線画像検出器モジュールの開発	日本放射線技術会　画像通信	30(2)	34-39	2007

DEVELOPMENT OF MULTI-ELEMENTAL MOLECULAR IMAGING ON SEMICONDUCTOR COMPTON TELESCOPE

Shinji Motomura, Yosuke Kanayama, Hiromitsu Haba, Kaori Igarashi, Yasuyoshi Watanabe and Shuichi Enomoto*

*Correspondence to: Shuichi Enomoto
Metallomics Research Unit, RIKEN
2-1, Hirosawa, Wako, Saitama, 351-0198, Japan
Tel. +81-48-467-9776; Fax: +81-48-467-9777
E-mail: semo@riken.jp

Abstract

The feasibility of using a Compton camera for multitracer imaging has been demonstrated with the results of two biological sample imaging experiments. The distribution of the multitracer administered to a soybean sample and a tumor-bearing mouse has been visualized for each nuclide simultaneously. Three-dimensional images of the multitracer have been obtained even though the samples were measured from a fixed direction.

Introduction

The multitracer, which was invented at RIKEN in 1991[1, 2], is a powerful tool for investigating the behavior of various chemical elements in a sample. It is produced by irradiating a metal target with a heavy-ion beam accelerated to an energy of 135 MeV/u, and then chemically processing the various radioactive nuclides produced mainly through nuclear-fragmentation reaction, into the final form such as multitracer solution. Since the multitracer contains the radioisotopes of various elements, the information regarding the radioisotopes under the same conditions can be obtained simultaneously by a single experiment. Moreover, the multitracer enables us to observe the correlated behavior among many elements. This information can never be obtained by combining the data of many single-tracer experiments. Owing to these advantages, the multitracer has found many applications in biology, medicine, environmental science, and other fields [3].

Although the potential advantages of multitracers are promising, no nondestructive inspection method has yet been established to realize their full potential particularly for in vivo imaging. This is because the multiple γ rays emitted from the multitracer span an energy range from ~100 keV to 2 MeV. For energies above ~300 keV, sufficient spatial resolution cannot be obtained by a conventional γ-ray imager equipped with mechanical collimators. In addition, the energy resolution must be high enough to distinguish each nuclide contained in the multitracer.

In this paper, we describe a prototype of a Compton camera for mutlitracer imaging, which we call GREI (Gamma-Ray Emission Imaging), and present some results of test experiments with biological samples. The original idea of the Compton camera was invented in the early 1970s [4], and it was soon proposed for medical imaging [5]. Since then, various types of Compton camera have been proposed for various uses [6].

Previously, we performed a test experiment using a Compton camera composed of two segmented germanium (Ge) detectors [7]. Owing to the excellent energy resolution of the Ge detectors, three γ-ray sources of ^{60}Co, ^{137}Cs and ^{152}Eu were clearly distinguished by setting energy windows on the corresponding γ-ray photo peaks, and their positions were simultaneously determined. The GREI system described in this paper has been modified taking into account the results of the test experiment, further simulations [8], and recent technologies developed for γ-ray detection [9]-[14].

Description of the GREI System

The GREI system is composed of two double-sided orthogonal-strip Ge detectors manufactured by Eurisys Mesures (Fig. 1). The detectors are arranged parallel to each other and mounted in a single cryostat. The dimensions of the active volume of the Ge crystals are 39 mm × 39 mm × 10 mm and 39 mm × 39 mm × 20 mm for the front and rear detectors, respectively. The strip pitch is 3 mm for both detectors. The center-to-center distance between the crystals is 60 mm.

The electronics are schematically shown in Fig. 2. Conventional circuit modules based on NIM and CAMAC standards are used. All the output signals of the preamplifiers are fed into the constant fraction discriminators (CFDs) through the timing filter amplifiers (TFAs), and the timing pulses are generated. All the timing pulses are fed into the time-to-digital converters (TDCs) to digitize the timing signals. To select the Compton scattering events, the timing pulses derived from the cathode strips are used to perform coincidence measurement between the front and rear detectors.

All the output signals of the preamplifiers are also fed into the shaping amplifiers to generate slow signals for energy measurement. Then the pulse heights are digitized by the analog-to-digital converters (ADCs).

In the current implementation, the transverse position of the γ-ray interaction is determined by a combination of the anode and cathode strips with the accuracy given by the width of the strip. On the other hand, the depth position of the γ-ray interaction in the Ge crystal can be determined more accurately than the thickness of the crystal, by taking into account the time difference between the signals from the anode and cathode strips [9]-[14]. To realize accurate

depth measurement, the time constants of TFAs were set to 500 ns and 60 ns for differentiation and integration, respectively. Delay time of the CFDs was set to 50 ns, which was the upper limit of the modules, and the fraction of the CFDs was set to 0.5.

The digitized data of the TDCs and ADCs are transferred event by event to the personal computer. The transferred data are analyzed on-line, and also recorded in list mode for further off-line analysis. If an incident γ ray is Compton scattered in the front detector and deposits energy E_1, and then the scattered γ ray is fully absorbed in the rear detector and deposits energy E_2, the original γ-ray energy E_γ is obtained by summing E_1 and E_2. Thus, the nuclides contained in the multitracer are distinguished by setting energy windows at the corresponding energy peaks in the E_γ spectrum. Throughout this paper, the range of an energy window was ± 5 keV of the peak position and the windows were applied in the software.

Implementation of Image Reconstruction Methods

For image reconstruction, we are currently employing a two-step method. In the first step, an intermediate image, which is called a simple back-projection (SBP) image, is constructed by simply accumulating the back-projections over all detected events, using an algorithm analogous to the cone-surface mapping algorithm [15]. The back-projection for one event is a cone surface that indicates the possible position of the γ-ray source. The cone axis is the straight line passing through the first and second interaction points. The half-cone angle θ is the Compton scattering angle determined by the following equation:

$$\cos\theta = 1 + m_e c^2 \left(\frac{1}{E_\gamma} - \frac{1}{E_\gamma - E_1} \right), \qquad (1)$$

where $m_e c^2$ is the rest-mass energy of an electron.

Here, we adopt a model that the SBP image is constructed by linear mapping of the source distribution image; that is,

$$n_i = \sum_j p_{ij} \lambda_j, \qquad (2)$$

where n_i is the value of voxel i in the SBP image, λ_j is the value of voxel j in the source distribution image, p_{ij} is the point-spread function (PSF), or the point kernel function [15], which represents the SBP image of the point source at

voxel j; the three-dimensional (3D) coordinates are represented by the single indices i and j. In general, the shape of the PSF varies depending on the source position, because the range of the accepted incident angle and scattering angle of γ rays depends on the source position. Therefore, a spatially variant PSF must be used to perform rigorous image reconstruction. However, the PSF should be approximated by a spatially invariant PSF within a local region.

Then the second step is to deconvolve the SBP image with the PSF. We have implemented an analytical algorithm and an iterative algorithm for the deconvolution.

If the PSF is assumed to be spatially invariant, λ_j can be reconstructed analytically by adopting the Fourier convolution theorem. The matrix p_{ij} is diagonalized by taking the Fourier transform of both sides of (2), and then λ_j is obtained in the spatial frequency domain as follows:

$$\lambda_j = \frac{n_j}{p_{jj}}. \qquad (3)$$

In most cases, an additional filter function (w_j) must be multiplied to the right side of (3) in order to suppress the statistical noise components, which are dominant in the high-frequency regions, that is:

$$\lambda_j = \frac{w_j n_j}{p_{jj}}. \qquad (4)$$

If a Wiener filter function can be designed for the system, (4) becomes the optimal estimation in terms of the least square errors. In addition, ad hoc filter functions, such as a Butterworth function, can be used for w_j to suppress the noise components in the high-frequency regions.

We have also implemented an iterative deconvolution algorithm, which was adapted from the additive SIRT algorithm [16]. First, an initial estimate of the original image $\lambda_j^{(0)}$ is obtained by averaging the SBP image:

$$\lambda_j^{(0)} = \frac{1}{N}\sum_{i=1}^{N} n_i. \qquad (5)$$

Then the (n+1)-th estimate ($\lambda_j^{(n+1)}$) is obtained from the n-th estimate ($\lambda_j^{(n)}$) as follows:

$$\lambda_j^{(n+1)} = \lambda_j^{(n)} + \sum_i \left(n_i - \sum_k \lambda_k^{(n)} p_{ik} \right) p_{ij}. \qquad (6)$$

Although spatially variant PSFs can be used for p_{ij}, spatially invariant PSFs have been used in the current work.

A close examination shows that (6) is the iteration term that minimize the square errors of the SBP image constructed from the estimated source distribution. This can be seen if we recast the steepest descent iteration term from [17]:

$$\begin{aligned}\Delta\lambda_j^{(n)} &= -\varepsilon\nabla\chi^2(\lambda_j^{(n)}) \\ &= -\varepsilon\frac{\sum_i \partial\left(n_i - \sum_k \lambda_k^{(n)} p_{ik}\right)^2}{\partial\lambda_j^{(n)}} \\ &= 2\varepsilon\sum_i\left(n_i - \sum_k \lambda_k^{(n)} p_{ik}\right)p_{ij},\end{aligned} \qquad (7)$$

where $\Delta\lambda_j^{(n)}$ is the displacement of the estimate in the iteration step, ε is a positive coefficient used to control the iteration. When ε=0.5, the second term on the right-hand side of (6) is obtained.

Since the PSF has a 3D distribution, 3D deconvolution must be performed in order to reconstruct 3D images. However, when the source distribution can be considered to be two-dimensional (2D), corresponding to the case of a sliced sample, 2D deconvolution is sufficient because there is no contamination from outside of the 2D plane. Thus, we have implemented both 2D and 3D deconvolution algorithms.

Performance of the Prototype

The absolute efficiencies for obtaining the full-energy γ-ray peaks from the sources 15 mm away from the center of the front detector are shown in Fig. 3, together with the values estimated by Monte Carlo simulation using a GEANT [18] code. The experimental values were derived from the experimental data mentioned in the next section. One can see that the GREI system has significant efficiency between the energy range from ~200 keV to ~2 MeV.

The effect of the statistical noise on the spatial resolution achieved with the prototype system was investigated in terms of the Fourier power spectral density (FPSD) of the SBP image. A point-like source of ^{65}Zn, which emits 1116 keV γ rays, was placed 69 mm away from the center of the front detector, and then three SBP images were constructed in 3D space with the detected event numbers of 1.0×10^4, 5.0×10^4, and 1.0×10^5. Then the SBP images were analytically deconvolved with the PSF constructed using a GEANT code. The full widths at half maximum (FWHMs) of the reconstructed images of the point source are shown in Table I for each number of events.

Experiment with Biological Samples

We have performed experiments with two biological samples in order to demonstrate the capability of nondestructive imaging of a multitracer. The first sample was a soybean plant administered with 310-kBq ^{137}Cs, 89-kBq ^{59}Fe, and 20-kBq ^{65}Zn. A photograph of the sample is shown in Fig. 10. The sample was fixed on a plane 15 mm away from the center of the front Ge detector. The measurement was carried out for 25 hours.

Fig. 4 shows the results of 2D imaging of the soybean sample. The energy windows were set at each peak position indicated in the γ-ray energy spectrum (Fig. 4(a)) to distinguish the radionuclides of ^{137}Cs, ^{59}Fe, and ^{65}Zn. The 2D SBP images were constructed for each nuclide on the plane where the sample was fixed, assuming a 2D distribution, and then the analytical reconstruction method was used to deconvolve the 2D SBP images with the 2D PSFs. The resulting images successfully visualized the different behaviors of the nuclides. The ^{137}Cs nuclide was distributed throughout the whole of the sample, because it is chemically analogous to K, while ^{59}Fe and ^{65}Zn remained near the root. The ^{65}Zn nuclide was found at the tip of the stem to some extent, where the plant was actively growing, because Zn is required for cell division.

In addition, we note that there is a difference in the background structure of the images. This is due to the difference in the number of events obtained for each nuclide; 2.5×10^6, 3.4×10^5, and 7.3×10^4 for ^{137}Cs, ^{59}Fe, and ^{65}Zn, respectively. The smaller the number of events, the larger the statistical noise component becomes, as mentioned in Section IV.

The second sample was a tumor-bearing mouse administered intravenously with a multitracer solution that includes 60-kBq ^{65}Zn, 30-kBq ^{59}Fe, and 10-kBq ^{88}Y. The sample was fixed on a board and placed just under the front detector, which was installed with its front face down. The measurement was carried out for 95 hours.

Fig. 5 shows the results of 2D imaging of the tumor-bearing mouse. As in the case of the soybean sample, the energy windows were set at each peak position indicated in the γ-ray energy spectrum (Fig. 8(a)) to distinguish the radionuclides of ^{65}Zn, ^{59}Fe, and ^{88}Y. Then the 2D SBP images were constructed for each nuclide on the 2D plane that intersects the tumor part, and the SBP images were analytically deconvolved with the 2D PSFs. The resulting images are only "focused" images along the assumed plane, because the other parts of the sample have some contribution to

the constructed 2D SBP images. Nevertheless, the accumulation of the nuclides in the tumor site was evident and ^{65}Zn was also found in the liver. The results are consistent with those reported in [19]-[21].

We have performed 3D imaging of these samples, even though the samples were measured from a fixed direction. When the sample is sufficiently close to the front detector, the source distribution can be projected towards various directions because no mechanical collimator is used. This is a distinctive feature of a Compton camera. First, the 3D SBP images were constructed in 3D space, then the SBP images were deconvolved with the 3D PSFs.

Fig. 6 shows the result of 3D imaging of ^{137}Cs in the soybean sample. The deconvolution was performed analytically. Since ^{137}Cs was distributed thoughout the whole sample, the shape of the sample can be recognized. However, there exists a warp in the reconstructed image, which may have been caused by the use of spatially invariant PSFs.

Fig. 7 shows the result of 3D imaging of ^{65}Zn in the tumor-bearing mouse. In this case, we could not obtain any satisfactory images by analytical deconvolution. Thus, the reconstructed space was limited to only the region around the sample, and the iterative deconvolution was performed. The resulting image successfully visualized the accumulation of ^{65}Zn in the tumor and the liver. However, the image has a similar warp to the 3D image of the soybean sample. Spatially variant PSFs should be incorporated to obtain more accurate images.

We were able to demonstrate the feasibility of using the GREI system for nondestructive imaging of multitracer. Recently, we were succeeded the real time metabolic imaging of three radioactive medicines simultaneously[22]. However, the measurement times taken to obtain the images would be unsuitable for practical imaging, although they can be shortened to about 10 hours if more intense γ-ray sources are used. Moreover, a higher spatial resolution would be desired to observe more fine structure. These demands would be met if the γ-ray tracking technique and pulse-shape analysis are implemented, which have been recently developed [23]. With these techniques implemented, the efficiency and the intrinsic characteristics are improved, thereby shortening the measurement time and improving the spatial resolution.

Summary

A prototype of a Compton camera, GREI, has been fabricated for nondestructive imaging of a multitracer. It is composed of two double-sided orthogonal-strip Ge detectors, and the efficiency is significant in the energy range

from ~200 keV to 2 MeV. The timing method was used to derive the depth position of the γ-ray interaction with a resolution of ~1 mm FWHM. Both analytical and iterative image reconstruction methods were implemented for 2D and 3D imaging. A test experiment was performed to demonstrate the capability of the GREI system. The resulting images successfully visualized the different behavior of each nuclide for both the soybean and the mouse sample. Furthermore, 3D images were obtained even though the samples were measured from a fixed direction. However, there was some distortion in the 3D images, which may have been caused by the use of spatially invariant PSFs. Spatially variant PSFs should be incorporated to obtain more accurate 3D images. To make the GREI system suitable for practical imaging, γ-ray tracking technique and pulse-shape analysis should be implemented.

Acknowlagement

This work was supported by the Grant-in-Aid for Scientific Research of the Ministry of Health, Labour and Welfare of Japan and by Grant for Nano Medicine Research of the New Enegy and Industrial Technology Development Organization of Japan. We thank Dr. R. Hirunuma and Dr. H. Takeichi for supporting the technical treatments.

References

[1] S. Ambe et al., "Preparation of a radioactive multitracer solution from gold foil irradiated by 135 MeV/nucleon ^{14}N ions," *Chem. Lett.* (1991) pp. 149-152.

[2] H. Haba, D. Kaji, Y. Kanayama, K. Igarashi, S. Enomoto. Radiochim. Acta. 93, 539-542 (2005).

[3] S. Enomoto, "Development of multitracer technology and application studies on biotrace element research," *Biomed. Res. Trace Elem.* 16, (2005) pp.233-240.

[4] V. Schönfelder et al., "A telescope for soft gamma ray astronomy," *Nucl. Instrum. Methods* 107, (1973) pp.385-394.

[5] R. W. Todd et al., "A proposed γ camera," *Nature* 251, (1974) pp.132-134.

[6] G. W. Phillips, "Gamma-ray imaging with Compton cameras," *Nucl. Instrum. Methods* B 99, (1995) pp.674-677

[7] Y. F. Yang et al., "A Compton Camera for Multi-tracer Imaging," *IEEE Trans. Nucl. Sci.* 48, (2001) pp.656-661.

[8] Y. F. Yang et al., "Monte Carlo simulations of the performance of a Compton camera consisting of position sensitive germanium detectors," *Nucl. Instrum. Methods* A 482, (2002) pp. 806-813.

[9] M. Momayezi et al., "Position resolution in a Ge-strip detector," *Proc. SPIE* 3768, (1999) pp. 530-537."

[10] M. Amman and P.N. Luke, "Three-dimensional position sensing and field shaping in orthogonal-strip germanium gamma-ray detectors," *Nucl. Instrum. Methods* A 452, (2000) pp.155-166.

[11] E. A. Wulf et al., "Depth measurement in a germanium strip detector," *IEEE Trans. Nucl. Sci.* 49, (2002) pp.1876-1880.

[12] E. A. Wulf et al., "Germanium strip detector Compton telescope using three-dimensional readout," *IEEE Trans. Nucl. Sci.* 50, (2003) pp.1182-1189.

[13] Motomura S, Enomoto S, Haba H, Igarashi K, Gono Y, Yano Y., Gamma-ray Compton imaging of multitracer in biological samples using strip germanium telescope, IEEE Trans. Nucl. Sci., 54, 710-717, (2007).

[14] Shigeto Kabuki, Kaori Hattori, Ryota Kohara, Etsuo Kunieda, Atsushi Kubo, Hidetoshi Kubo, Kentaro Miuchi, Tadaki Nakahara, Tsutomu Nagayoshi, Hironobu Nishimura, Yoko Okada, Reiko Orito, Hiroyuki Sekiya Takashi Shirahata, Atsushi Takada, and Kazuki Ueno, Development of Electron Tracking Compton Camera using micro pixel gas chamber for medical imaging, Nucl. Inst. Meth. A, 580, (2007), pp. 1031-1035.

[15] R. C. Rohe et al., "The Spatially-Variant Backprojection Point Kernel Function of an Energy-Subtraction Compton Scatter Camera for Medical Imaging," *IEEE Trans. Nucl. Sci.* 44, (1997) pp. 2477-2482.

[16] P. Gilbert, "Iterative methods for the three-dimensional resonstruction of an object from projections," *J. Theor. Biol.* 36, (1972) pp.105-117.

[17] W. H. Press, S. A. Teukolsky, W. T. Vetterling, and B. P. Flannery, *Numerical Recipes in C: The Art of Scientific Computing,* 2nd ed., Cambridge: Cambridge University Press, 1992, p. 681.

[18] GEANT, *Detector Description and Simulation Tool* (CERN, Geneva, 1993).

[19] H. Tamano et al.: "Tumor accumulation of radioactive trace elements: a multitracer study," *Biomed. Res. Trace Elements* 12, (2001) pp. 96-101.

[20] H. Tamano et al.: "Preferential uptake of zinc, manganese and rubidium in rat brain tumor," *Nucl. Med. Biol.* 29, (2002) pp. 505-508.

[21] A. Takeda, H. Tamano, S. Enomoto, N. Oku. "Zinc-65 imaging of rat brain tumors," *Cancer Res.* 61, (2001) pp. 5065-5069.

[22] Motomura et al., *JAAS*, submitted.

[23] K. Vetter et al: "Gamma-ray imaging with position-sensitive HPGe detectors," *Nucl. Instrum. Methods* A 525, (2004) pp. 322-327.

Figures and Table

Figure 1. Schematic of the strip Ge telescope operated as a Compton camera.

Figure 2. Circuit diagram of the current prototype of the GREI system. The circuit modules are based on NIM and CAMAC standards.

Figure 3. Absolute efficiencies for obtaining the full-energy γ-ray peaks.

Figure 4. Results of 2D imaging of the soybean sample.

Figure 5. Results of 2D imaging of the tumor-bearing mouse.

Figure 6. Three-dimensional image of ^{137}Cs distributed in the soybean sample. A photograph of the sample is also shown at the center.

Figure 7. Three-dimensional image of ^{65}Zn distributed in the tumor-bearing mouse. The orientations of the sample are indicated by the mouse figures.

Table 1. Spatial resolution of the reconstructed image and derived transient spatial frequency of the FPSD of the SBP image.

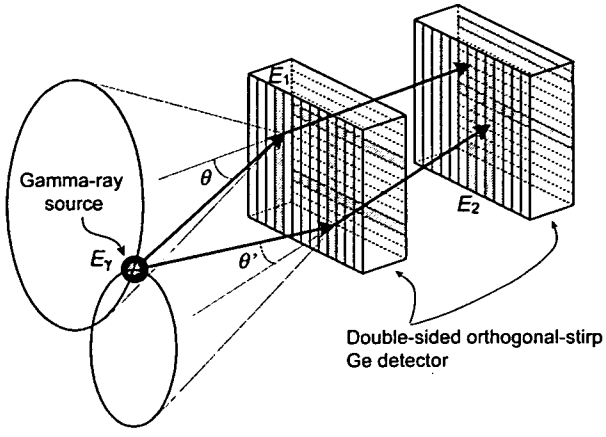
Gamma-ray
source
E_γ
θ
θ'
E_1
E_2
Double-sided orthogonal-stirp
Ge detector

Fig. 1.

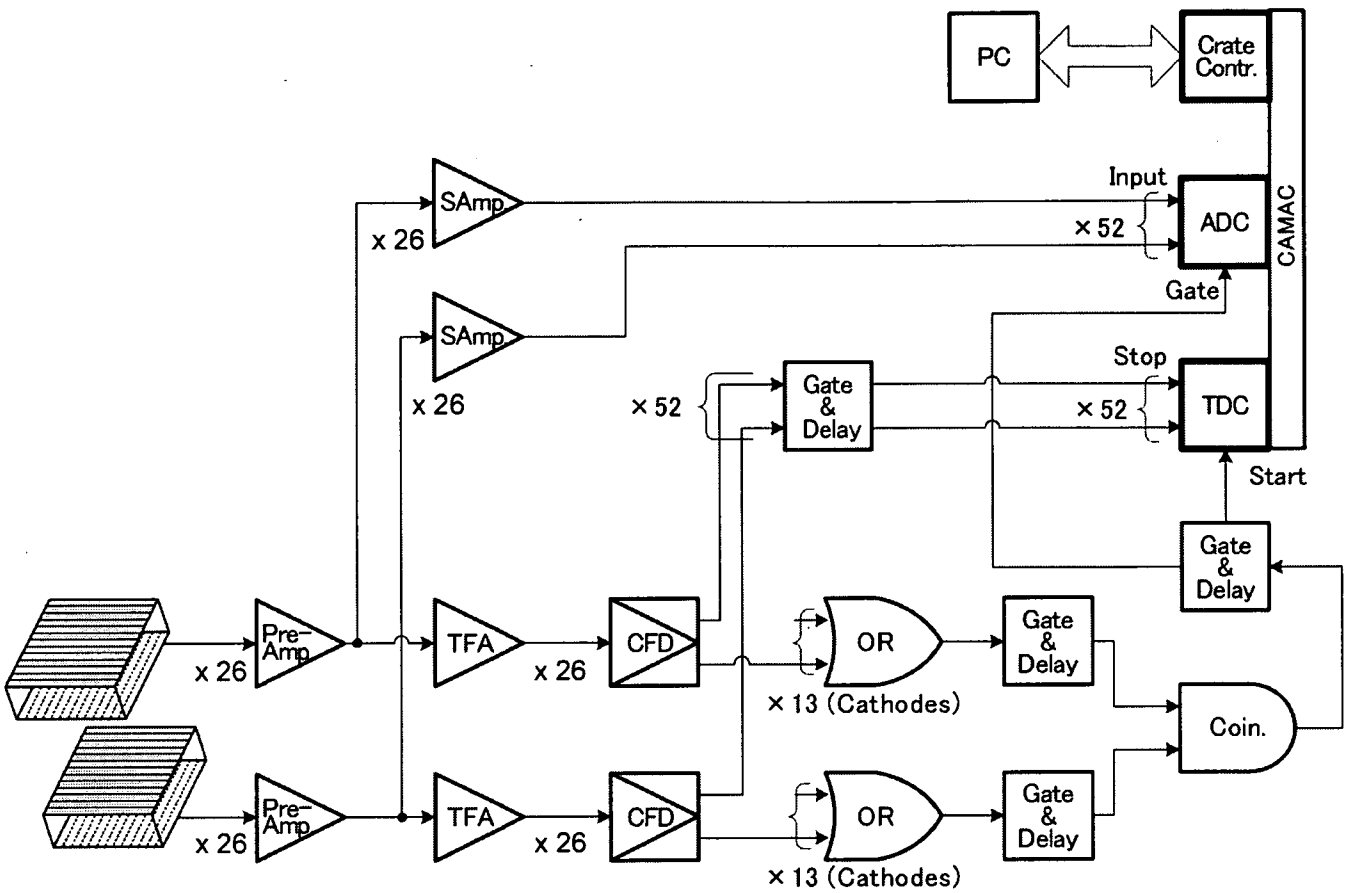
PC
Crate Contr.
CAMAC
Input
SAmp
x 26
x 52
ADC
Gate
SAmp
x 26
Stop
x 52
Gate & Delay
x 52
TDC
Start
Gate & Delay
Pre-Amp
x 26
TFA
x 26
CFD
OR
Gate & Delay
x 13 (Cathodes)
Coin.
Pre-Amp
x 26
TFA
x 26
CFD
OR
Gate & Delay
x 13 (Cathodes)

Fig. 2.